# Semiclassical modeling of Rydberg wave-packet dynamics in diatomic molecules: Average decoupling theory

S. N. Altunata, J. Cao, and R. W. Field*
*Department of Chemistry, Massachusetts Institute of Technology, Cambridge, Massachusetts 02139*
(Received 12 November 2001; revised manuscript received 11 February 2002; published 10 May 2002)

The semiclassical dynamics of Rydberg electronic wave packets in diatomic molecules is investigated using a sum over classical trajectories method, which is based on the semiclassical form of Feynman's path integral. Our approach allows us to calculate intramolecular energy redistribution rates based on averaging of coupling parameters over classical trajectories associated with time-dependent parts of the overall system that exhibit different periodicities. The accuracy of our method is tested against perturbation theory and good agreement is obtained. A resonance structure in the computed autocorrelation function has also been observed in the case of rotating nuclei, when the periods of the classical trajectories of the electron match an integer multiple of the rotational period. This has previously been called the ''stroboscopic'' effect.

DOI: 10.1103/PhysRevA.65.053415 PACS number(s): 33.80.Rv

## I. INTRODUCTION

Rydberg wave-packet dynamics in diatomic systems is an interesting subject from experimental and theoretical points of view. This arises from the fact that in the limit of high principal quantum number $n$ electronic orbit periods become comparable to vibrational and rotational periods of the nuclei. This results in the reduction of the Born-Oppenheimer picture to the status of a crude approximation. Several theories [2,3] have been developed to correct for these nonadiabatic effects, based on the formalisms of the variational principle and scattering theory. However, in a time-dependent approach, evidence from experiment [4] with regard to observed recurrences at the classical periods of the system in the measured autocorrelation function of a Rydberg wave packet suggests that a semiclassical method might provide insights that are not immediately accessible by the previous treatments.

Our semiclassical model rests on the observation that when the electron is excited to a Rydberg state it starts to exchange energy with the ion core much like the components of a system of coupled pendula and springs. As a result of the electronic excitation, the expectation value of the electron distance from the origin in the molecular frame is suddenly increased to a value several times larger than the molecular size and the electron transfers energy and momentum to the internal states of the diatom primarily through long range electrostatic interactions.[1] Since the ion core is in general not spherical, these interactions are not spherically symmetric and the Hamiltonian is off diagonal in products of electronic and rovibrational basis states.

There are parallels between this situation and the classical problem of a pendulum coupled to a linear spring in the earth's gravitation field (Fig. 1).

In general, the trajectories of the pendulum-spring system are not analytically solvable and one must approach the problem numerically [5]. However, if the natural frequency of the pendulum is much larger than the natural frequency of the mass-spring system, then the equations of motion can be separated using the adiabatic approximation in which the trajectory for the pendulum is solved for, given a fixed extension or compression of the spring. One can *correct* for the adiabatic approximation by replacing the time-dependent tension force applied by the spring-mass system on the pendulum by an average value over one period of the independent oscillation of the spring-mass system, as opposed to assuming that the spring-mass system is ''frozen'' with respect to the motion of the pendulum. It should be noted here that this argument could equally well be applied to the opposite limiting case where the natural frequency of the oscillator exceeds the natural frequency of the pendulum.

In the sections that follow we use the same ideas developed in the pendulum-spring example to analyze the dynamics of a well localized Rydberg wave packet in a homonuclear diatomic molecule. Our fundamental theoretical tool is a sum over classical trajectories formula that was obtained first by Mallalieu and Stroud [1] for the hydrogen atom by applying a stationary phase to Feynman's path integral. Due to its semiclassical nature, this formula is accurate for high values of the relevant quantum numbers of the problem. In

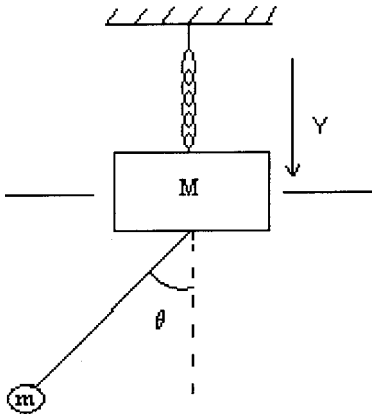


FIG. 1. Coupled pendulum-spring system.

*Author to whom correspondence should be addressed.

[1]We neglect the electrodynamic interactions, as corrections can be obtained using perturbation theory.

 

particular, this restricts the choice of principal quantum number for the electronic motion to be above a certain threshold, which we have determined to be $\bar{n}=7$. This makes the electronic frequency smaller than a typical vibrational frequency for a diatomic molecule. Hence, when vibrational-electronic couplings are considered, the electron will be taken to be the slow moving part of the system and the adiabatic approximation as applied to the motion of the electron will get corrected, as in the oscillator-pendulum example. It is, however, possible to investigate the rotational-electronic couplings when the frequencies of the two motions are comparable. Therefore two cases will be analyzed for this situation; one for the case of very slow electronic motion in comparison to rotational motion ($\omega_{el} \ll \omega_{rot}$) and one for the case where the electronic frequency is near the rotational frequency. As will be demonstrated, stroboscopic effects are recovered between the two motions in this limit when the rotational frequency is chosen to be twice the electronic frequency. These effects can be considered to be quantum mechanical manifestations of the classical concept of resonance.

## II. THEORY

The starting point is the propagator that gives the time evolution of an arbitrary wave packet for a given Hamiltonian. The propagator is defined by

$$K(\vec{x}_f,t_f,\vec{x}_i,t_i)=\langle \vec{x}_f,t_f|\vec{x}_i,t_i\rangle=\langle \vec{x}_f|e^{-\frac{i\hat{H}(t_f-t_i)}{\hbar}}|\vec{x}_i\rangle, \quad (1)$$

where $\hat{H}=\hat{p}^2/2m+V(\vec{r})$. Hence for an initial wave packet defined by $\Psi(\vec{x}_i,t_i)$, the wave packet evaluated at $(\vec{x}_f,t_f)$ is given by

$$\Psi(\vec{x}_f,t_f)=\int K(\vec{x}_f,t_f,\vec{x}_i,t_i)\Psi(\vec{x}_i,t_i)d\vec{x}_i. \quad (2)$$

Feynman's well known analytical formula for the propagator is

$$K(\vec{x}_f,t_f,\vec{x}_i,t_i)=\int D(\vec{x}(t'))e^{\int L(\vec{x}(t'))dt'}. \quad (3)$$

Here $L$ is the classical Lagrangian evaluated on the primed path $\vec{x}(t')$ that connects $\vec{x}_f$ and $\vec{x}_i$ and is given by

$$L=T-V=\frac{p^2}{2m}-V(\vec{r}). \quad (4)$$

$D$ represents an integration over all possible paths between $\vec{x}_f$ and $\vec{x}_i$. When stationary phase is applied to this integral form, we get the condition $\delta L=0$, which is equivalent to Newton's equations of motion. This suggests that the dominant contribution to the Feynman propagator comes from classical trajectories that connect $\vec{x}_f$ and $\vec{x}_i$. After proper transformation is applied, we arrive at the Gutzwiller semiclassical form [6] for the propagator:

$$K(\vec{x}_f,t_f,\vec{x}_i,t_i)=\left(\frac{1}{2\pi i\hbar}\right)^{N/2}\sum_j \left|\det\frac{\partial^2 R_j(\vec{x}_f,\vec{x}_i,t)}{\partial\vec{x}_f\partial\vec{x}_i}\right|^{1/2} \times e^{(R_j i/\hbar - i\pi\mu_j/2)}, \quad (5)$$

where $R_j$ is the action for the $j$th classical trajectory given by

$$R_j(\vec{x}_f,\vec{x}_i,t)=\int_0^t L(\vec{x}_j(t'))dt', \quad (6)$$

and $\mu_j$ is the number of conjugate points along the same trajectory,[2] which can be determined from the relation

$$e^{i\pi\mu_j}=\frac{\det(\partial^2 R_j/\partial\vec{x}_f\partial\vec{x}_i)}{\det|\partial^2 R_j/\partial\vec{x}_f\partial\vec{x}_i|}. \quad (7)$$

In our applications we will be concerned with many-body systems. For such a case, the classical trajectory $\vec{x}(t')$ becomes the system trajectory vector with components corresponding to generalized coordinates. The time derivative of this vector gives us the conjugate momenta as functions of time. The common notation to describe a system with $N$ degrees of freedom is a system vector $\vec{x}^N(t)$, which signifies the $N$ generalized coordinates that describe the overall time evolution.

The autocorrelation function is defined by

$$c(t)=\langle\psi(\vec{r},0)|\psi(\vec{r},t)\rangle \quad (8)$$

for a wave function $\psi$ evolving under a Hamiltonian $\hat{H}(\vec{p},\vec{r})$. In integral form,

$$c(t)=\int\int \psi^*(\vec{r}_f,0)\psi(\vec{r}_i,0)K(\vec{r}_f,\vec{r}_i,t)d\vec{r}_f d\vec{r}_i. \quad (9)$$

To proceed with the derivation we make the crucial assumption that the initial wave packet is well localized in the *semiclassical* variables. Then the amplitude $\psi^*(\vec{r}_f,0)\psi(\vec{r}_i,0)$ for $\vec{r}_f\neq\vec{r}_i$ will be small. Hence we can approximate $c(t)$ by replacing the integration over $d\vec{r}_i$ by a constant value of the initial position wave function evaluated at $\vec{r}_f=\vec{r}_i$ and write

$$c(t)\approx\int|\psi(\vec{r},0)|^2K(\vec{r},\vec{r},t)dt = \mathrm{Tr}[\psi^*(\vec{r}_f,0)K(\vec{r}_f,\vec{r}_i,t)\psi(\vec{r}_i,0)]. \quad (10)$$

Further, assuming that $\psi^*(\vec{r}_f,0)\psi(\vec{r}_i,0)$ is not oscillatory, we can impose stationary phase on the propagator to get

[2]For a clear explanation of the conjugate points and their physical meaning, see [6].

$$\frac{\partial K}{\partial \vec{r}_i}\frac{\partial \vec{r}_i}{\partial \vec{r}_f}+\frac{\partial K}{\partial \vec{r}_f}=0,$$

which gives

$$-\vec{p}_i+\vec{p}_f=0. \tag{11}$$

With the additional condition that $\vec{r}_f=\vec{r}_i$, this becomes the definition of a periodic orbit. Thus, from the sum over classical trajectories, only trajectories located near periodic closed orbits will contribute to the integral. It is allowed that the trajectories will have completed multiple periods by the time at which the autocorrelation function is evaluated. Thus, it is sensible to label each periodic orbit by an integer $k$, the number of cycles completed at $t$. Next, we choose a point $\vec{r}_0$ on the periodic orbit which lies in a region where the initial wave packet has significant amplitude, and we expand the phase of the propagator to second order about this point:

$$R=R_k(\vec{r}_0,\vec{r}_0,t)+\frac{1}{2}\sum_{i,j=1}^{N} I_{ij}(r^i-r_0^i)(r^j-r_0^j). \tag{12}$$

Here,

$$I=\left(\frac{\partial^2 R}{\partial \vec{r}_f\partial \vec{r}_i}+\frac{\partial^2 R}{\partial \vec{r}_i\partial \vec{r}_f}+\frac{\partial^2 R}{\partial \vec{r}_f\partial \vec{r}_f}+\frac{\partial^2 R}{\partial \vec{r}_i\partial \vec{r}_i}\right)\Bigg|_{\vec{r}_i=\vec{r}_f=\vec{r}_0}. \tag{13}$$

Thus the autocorrelation function can be written as

$$c(t)=\left(\frac{1}{2\pi i\hbar}\right)^{N/2}\sum_k\left(\det\left|\frac{\partial^2 R}{\partial \vec{r}_f\partial \vec{r}_i}\right|\right)^{1/2}\Bigg|_{\vec{r}_0} e^{-(i/\hbar)R_k}\times\int|\psi(\vec{r},0)|^2 e^{-(i/2\hbar)\sum_{i,j=1}^{N} I_{ij}(r^i-r_0^i)(r^j-r_0^j)}d\vec{r}. \tag{14}$$

This expression is subject to the restriction that $\vec{r}_f=\vec{r}_i$. We can improve on the approximation by distinguishing the two points but retaining the same form:

$$c(t)=\left(\frac{1}{2\pi i\hbar}\right)^{N/2}\sum_k\left(\det\left|\frac{\partial^2 R}{\partial \vec{r}_f\partial \vec{r}_i}\right|\right)^{1/2}\Bigg|_{\vec{r}_o} e^{-(i/\hbar)R_k}\times\int\int\psi(\vec{r}_f,0)^*\psi(\vec{r}_i,0)e^{-(i/\hbar)I(\vec{r}_f,\vec{r}_i)}d\vec{r}_f d\vec{r}_i, \tag{15}$$

with

$$I(\vec{r}_f,\vec{r}_i)=\frac{\partial R}{\partial \vec{r}_i}\cdot(\vec{r}_i-\vec{r}_0)+\frac{\partial R}{\partial \vec{r}_f}\cdot(\vec{r}_f-\vec{r}_0)+\frac{1}{2}(\vec{r}_i-\vec{r}_0)\cdot\frac{\partial^2 R}{\partial^2 \vec{r}_i}\cdot(\vec{r}_i-\vec{r}_0)+\frac{1}{2}(\vec{r}_f-\vec{r}_0)\cdot\frac{\partial^2 R}{\partial^2 \vec{r}_f}\cdot(\vec{r}_f-\vec{r}_0)+(\vec{r}_f-\vec{r}_0)\cdot\frac{\partial^2 R}{\partial \vec{r}_f\partial \vec{r}_i}\cdot(\vec{r}_i-\vec{r}_0), \tag{16}$$

and the period of the periodic orbit $k$ passing through $\vec{r}_0$ is given by $T_{po}=t/k$.

In general, molecular $N$-body systems will have two or more dynamical variables, corresponding to generalized coordinates, which will evolve over time scales that exhibit different periods. However, these dynamical variables will be coupled through electrostatic interactions and therefore will exchange momentum. The above analysis invites us to approach this problem in complete analogy to the oscillator-pendulum problem described in the Introduction. *We will decouple the interaction by an average over a periodic trajectory of one part of the system, thereby obtaining an analytical expression for the autocorrelation function.* Within this framework we are further allowed to use an approximate, trajectory-dependent potential function instead of the full potential felt by the wave packet, since the autocorrelation function has been put in a form that is an explicit sum of the classical periodic orbits and therefore it is the evolution of these periodic orbits that plays the key role in the final result.

In the case that there are two parts of the overall system that evolve on different time scales, such an average will lead to the separation of the actions $R$ in the following manner:

$$R_{tot}=R_k^1+R_2^k, \tag{17}$$

implying that the second part evolves in averaged correlation with the first part through its particular periodic orbit $k$, leading to an autocorrelation function given by

$$c(t)=\sum_k a_k e^{(i/\hbar)R_k^1}, \tag{18}$$

where $a_k$ is a complex number to be determined and contains the phase-amplitude contribution of the second part.

In the next section we apply the outlined method to a nonrotating diatomic system where vibrational degrees of

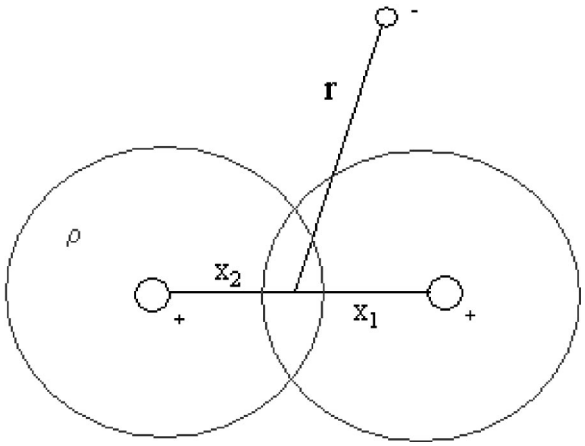


FIG. 2. Diatomic molecule: $U=X_1-X_2; P=X_1+X_2$.

freedom are coupled to the electronic motion through a quadrupole interaction. The accuracy of the autocorrelation function is then compared with a perturbation theory calculation. In Sec. IV we add in rotations to our calculations and demonstrate how the resonances between the electronic and the rotational motions manifest themselves in the survival probability.

### III. VIBRATIONAL COUPLING

We investigate the time evolution of a well localized wave packet for a $H_2$ like system with an infinite barrier against rotation.

In Fig. 2 we have an orbiting Rydberg electron, two nuclei of equal charge $+1$, and an effective charge density $\rho(\vec{r}')$, which is responsible for holding the nuclei together. We define, in atomic units,

$$V(\vec{r})=\int \frac{\rho(\vec{r}')}{|\vec{r}-\vec{r}'|}d\vec{r}',$$

$$U=X_1-X_2,$$

$$P=X_1+X_2. \tag{19}$$

By describing the inner electron as a static charge density, we are discarding any dynamics due to a possible excitation from the core ground electronic state via exchange of energy with the Rydberg electron. This is a good approximation if the Rydberg wave packet is localized sufficiently far from the core, as will be the case in our model. Neglecting free translation, we can write the Lagrangian of the system as

$$L=\frac{1}{2}\mu\dot{R}^2+\frac{1}{2}[\dot{r}^2+r^2\dot{\theta}^2+r^2\sin(\theta)^2\dot{\phi}^2]+\frac{1}{r_1}$$

$$+\frac{1}{r_2}+D_e-\frac{1}{2}k_{eff}R^2-V(\vec{r}), \tag{20}$$

where $R=U-U_{eq}$, $\mu=M_{proton}/2$, $D_e$ is the depth of the potential energy curve for the ionic diatom, and $k_{eff}$ is a parameter determined from the curvature of the potential energy curve at the minimum, $U=U_{eq}$. Anharmonic terms are neglected in the nuclear potential and consequently the results we obtain will be valid only for low lying vibrational states. From molecular orbital theory we can take the following form for the charge density:

$$\rho(\vec{r}')=|1\sigma s|^2=\frac{1}{2(1+S)}[1s_A(\vec{r}')+1s_B(\vec{r}')]^2, \tag{21}$$

where $S$ is the overlap integral given by

$$S=\int 1s_A(\vec{r}')^*1s_B(\vec{r}')d\vec{r}'. \tag{22}$$

The accuracy of the method outlined in Sec. II depends on whether the initial wave packet that will evolve subject to this Lagrangian is sufficiently localized. Thus we consider an initial Rydberg wave packet that is localized near the uncertainty limit in all three electronic coordinates [7]. Our initial wave packet is defined by

$$\psi(\vec{x},0)=\psi_{el}(\vec{r},0)\psi_{nuc}(R),$$

$$\psi_{el}(\vec{r},0)=\sum_n \left(\frac{1}{\pi\sigma_n^2}\right)^{1/4} e^{-(n-\bar{n})^2/2\sigma_n^2}\phi_{n,n-1,n-1},$$

$$\psi_{nuc}(R)=\sqrt{\frac{1}{3}}(\psi_0^{HO}+\psi_1^{HO}+\psi_2^{HO}), \tag{23}$$

where $\phi_{n,n-1,n-1}$ is a hydrogenic wave function,[3] with principal quantum number $n$, orbital angular quantum number $n-1$, magnetic quantum number $n-1$, and $\bar{n}=7$ with $\sigma_n \ll \bar{n}$. The wave functions labeled $HO$ refer to the first three harmonic oscillator eigenstates. This choice is made to account for the possibility of vibrational transitions and the resultant dynamics. Electron exchange is neglected because the overlap of the Rydberg wave packet with the ground electronic wave function of the core is small, spin-orbit coupling is also ignored. An approximate expression for the hydrogenic linear combination that appears in Eq. (23), using spherical polar coordinates, is given in [8], which shows that the wave packet is localized about

$$\bar{r}=\bar{n}^2, \quad \bar{\theta}=\frac{\pi}{2}, \quad \bar{\phi}=0. \tag{24}$$

This describes an electronic wave packet confined to the $x$-$y$ plane at a large average distance from the origin. Furthermore, the linear combination consists exclusively of high $l$'s, which imposes a large centrifugal barrier against electron penetration toward the center of the ion-core. In particular, one can safely assume that the classical trajectories of Sec. II, which will ultimately sum to yield the autocorrelation function, will lie in an asymptotic region. The potential ex-

[3]This electronic wave packet is convenient to use as a theoretical tool but is not meant to be a model for an experimentally realizable physical system.

perienced by such classical trajectories can be described by a static multipole expansion. The electron-electron interaction in this limit becomes

$$V(\vec{r})=\int \frac{\rho(\vec{r}')}{|\vec{r}-\vec{r}'|}d\vec{r}'=\sum_l \int_0^r \rho(\vec{r}')p_l(\vec{r}\cdot\vec{r}')\frac{(r')^l}{r^{l+1}}dv' + \sum_l \int_r^\infty \rho(\vec{r}')p_l(\vec{r}.\vec{r}')\frac{r^l}{(r')^{l+1}}dv'. \quad (25)$$

For sufficiently large $r$ we can assume that this expression is near its asymptotic limit, approximately giving

$$V(\vec{r})=\frac{1}{r}. \quad (26)$$

We want to investigate the effect of nuclear dynamics on the electronic motion and thus we expand the nuclear attraction to its first nonvanishing multipole term that includes the internuclear distance. Since the initial electronic wave function lies in the $x$-$y$ plane, a natural choice of trajectories for Eq. (18) is those confined to the same plane and which lie in the asymptotic region. Multipole expansion to second order reveals

$$\frac{1}{r_1}+\frac{1}{r_2}\approx\frac{1}{r}\left(2-\frac{[1-3\cos^2(\phi)]U^2}{4r^2}\right), \quad (27)$$

where $\phi$ is the planar azimuthal angle. Here the appearance of the quadrupole term $[1-3\cos^2(\phi)]U^2/r^3$ breaks the spherical symmetry and angular momentum is no longer conserved. As in the pendulum-spring example, we decouple this asymmetry from the electronic degrees of freedom and couple it completely to nuclear motion by introducing a time-modulated force constant $\overline{g_{po}}(t)$ as the average value of the quadrupole term along a periodic trajectory of the electron. Explicitly, we define

$$\overline{g_{po}^{(t)}}=\frac{1}{T_{po}}\oint\frac{1-3\cos^2[\phi(t')]}{2r(t')^3}dt'+k_{eff}. \quad (28)$$

The Lagrangian now becomes

$$L^{po}=\frac{1}{2}\mu\dot{R}^2+\frac{1}{2}[\dot{r}^2+r^2\dot{\theta}^2+r^2\sin(\theta)^2\dot{\phi}^2]+\frac{1}{r}+D_0-\frac{1}{2}\overline{g_{po}^{(t)}}\left(R+\frac{U_{eq}(\overline{g_{po}^{(t)}}-k_{eff})}{\overline{g_{po}^{(t)}}}\right)^2-\frac{k_{eff}}{2\overline{g_{po}^{(t)}}}U_{eq}^2(\overline{g_{po}^{(t)}}-k_{eff}), \quad (29)$$

and the evaluation along a periodic trajectory of the electron in the pure Coulomb potential is evident. This is the Kepler problem and the solutions are the Kepler ellipses, as we have anticipated. We let $\overline{g_{po}^{(t)}}=\mu\omega_k^2$ with the electronic period given by $T=t/k$. Along the periodic trajectory the actions for the nuclei and the electron separate and so do the semiclassical propagators. From Eq. (15) we get

$$c(t)=\sum_k a_k e^{iR_k^{el}}\int\psi_{nuc}^*(R)K^k(R,R',t)\times\psi_{nuc}(R')dRdR'. \quad (30)$$

The complex number $\Omega(k)=a_k e^{iR_k^{el}}$ is obtained from circular trajectories in a pure spherical Coulomb interaction and its explicit form is available in [1]. For a circular orbit of period $t/k$ we have

$$\phi(t')=\frac{2\pi k t'}{t}+\overline{\phi} \quad (31)$$

and Kepler's law leads to

$$r(t)=\left(\frac{t}{2\pi k}\right)^{2/3}. \quad (32)$$

Evaluation of $w_k$ along such circular trajectories, using Eq. (28), gives

$$w_k=\sqrt{\frac{-k^2\pi^2/t^2+k_{eff}}{\mu}}. \quad (33)$$

Within the adiabatic picture the angular frequency $w_k$ would simply be given by $\sqrt{k_{eff}/\mu}$. The term $-k^2\pi^2/t^2$ is the *correction* we have obtained by explicitly considering the coupling between electronic and nuclear degrees of freedom. We can go one step further and write an analytical expression for the autocorrelation function in analytical form using the exact propagator for the harmonic oscillator:

$$c(t)=\sum_k \Omega(k)\int\sqrt{\frac{\mu\omega_k}{2\pi i\sin(\omega_k t)}}\exp\left(\frac{im\omega_k}{2\sin(w_k t)}\times[(R^2+R'^2)\cos(\omega_k t)-2RR')]\right)\times\psi^*(R)\psi(R')dRdR'. \quad (34)$$

This is valid for any vibrational wave packet $\psi_{nuc}(R)$ excited at time $t=0$ and contains all information about the coherence between the zero-order states. For our initial wave packet the survival probability can be written as

$$|c(t)|^2=\sum_{n=1}^3\sum_{n'=1}^3\sum_k\sum_{k'}a_{nn'}\Omega(k,k')\times e^{i[(n+1/2)\omega_k-(n'+1/2)\omega_{k'}]}. \quad (35)$$

This is further separated as

$$
\begin{aligned}
&|c(t)|^2 \\
&= \sum_k |\Omega(k)|^2 + \sum_n \sum_{k \neq k'} a_n \Omega(k,k') e^{i[(n+1/2)(\omega_k - \omega_k')]} \\
&+ \sum_{n \neq n'} \sum_k a_{nn'} \Omega(k) e^{i[(n-n')(\omega_k)]} \\
&+ \sum_{n \neq n'} \sum_{k \neq k'} a_{nn'} \Omega(k,k') e^{i[(n+1/2)\omega_k - (n'+1/2)\omega_{k'}]}.
\end{aligned} \tag{36}
$$

$\Sigma_k \Omega(k)$ is an *atomic* term, which leads to the autocorrelation function for the hydrogen atom. The remaining terms in Eq. (36) contain all the molecular information. This form tells us that, at the hydrogen atom recurrence times, all the molecular information, which is given by the remaining terms in Eq. (36) when the atomic term is taken out, disappears, since the recurrence time implies that the *atomic* term is equal to 1. Thus, an atomic signature is built into the molecular recurrence spectrum within this framework.

### Perturbation analysis

Given that most of the amplitude of the initial wave function lies outside the core region, little error is introduced if the asymptotic form of the potential is used over all space. This facilitates a perturbation theory treatment of the same problem, which we present now. The autocorrelation function in general is given by

$$
c(t) = \sum_{n,v} |a_n|^2 e^{-iE_{n,l,v}t}, \tag{37}
$$

where the $|a_n|$ are the amplitudes of the zero-order states, $n$ and $l$ are the electronic quantum numbers, and $v$ is the vibrational quantum number. According to first-order perturbation theory,

$$
E_{n,l,v} = E^0_{n,v} + E^1_{n,l,v}, \tag{38}
$$

with

$$
\begin{aligned}
E^0_{n,v} &= -\frac{1}{2n^2} + \sqrt{\frac{k_{eff}}{\mu}}\left(v + \frac{1}{2}\right) - D_e, \\
E^1_{n,l,v} &= \left\langle n,l,m,v \left| \frac{[1 - 3\cos^2(\phi)]U^2}{4r^3} \right| n,l,m,v \right\rangle.
\end{aligned} \tag{39}
$$

When the matrix elements are calculated we get

$$
E_{n,l,v} = \left(\frac{-1}{8}\right) \frac{1}{l(l+1/2)(l+1)n^3} \left(\frac{v+1/2}{\sqrt{k_{eff}\mu}} + Ueq^2\right) \tag{40}
$$

as the corrections to the zero-order energies. The autocorrelation function computed from perturbation theory is compared to the result from average decoupling theory in Fig. 3.

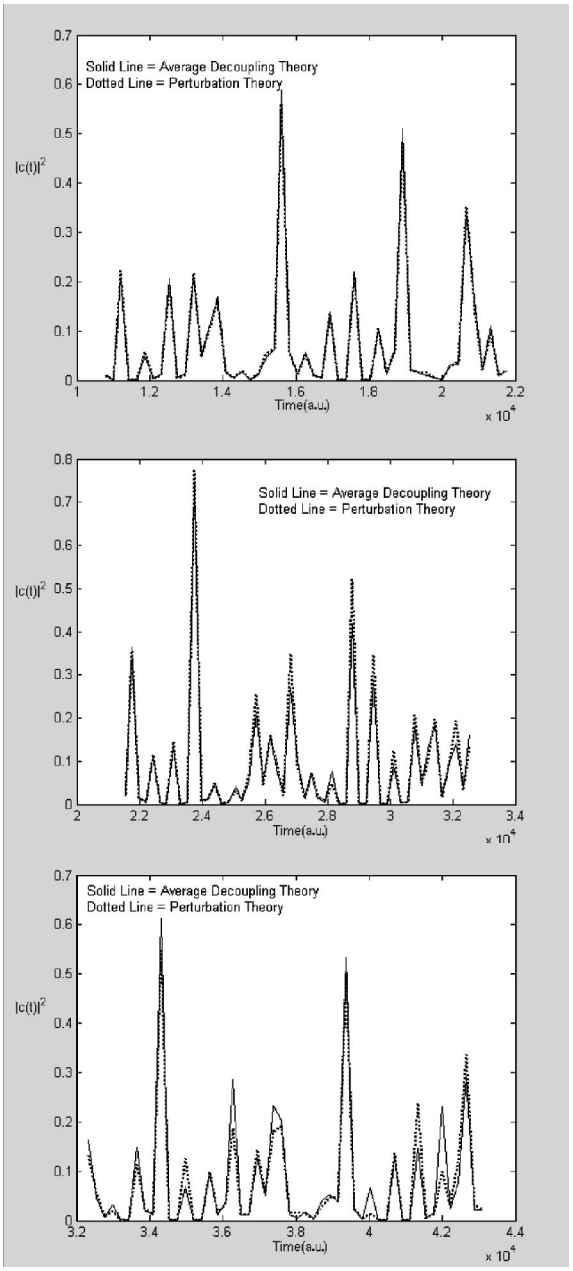


FIG. 3. Theoretical survival probability. The solid line is average decoupling theoryand the dashed line is perturbation theory. The parameters used are $\sigma_n = 10/(2\pi)$, $\bar{n} = 7$, $k_{eff} = 0.334$, $\mu = 918.01$, $D_e = 0.102$, $U_{eq} = 2$, $v = 0,1,2$.

The numerical values of the force constants and the potential energy curve depths are those for $H_2^+$. It is seen that the two theories agree quite well even until very late times. Only after about 15 classical electronic periods, given by $T_{cl} = 2\pi\bar{n}^3$, do the amplitudes start to differ.

### Fourier transform spectrum

The Fourier transform of the autocorrelation function gives the energy spectrum of the core plus electron system. In Fig. 4 we have plotted the Fourier transform of the autocorrelation function that was computed using average decou-

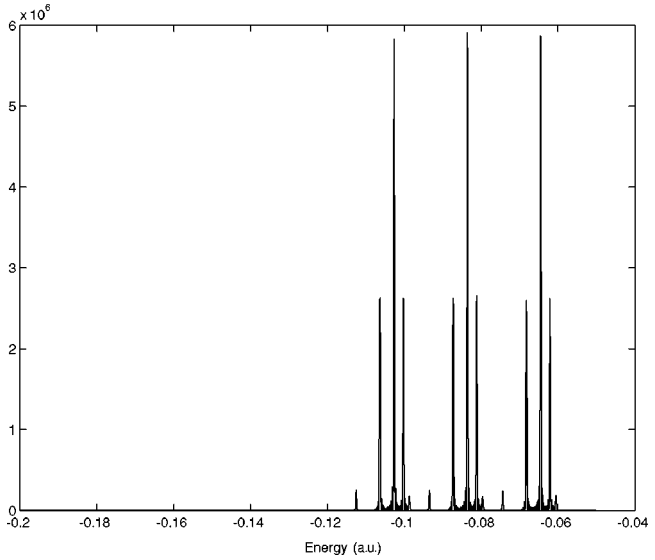


FIG. 4. Fourier transform spectrum. The three lines correspond to Rydberg series converging to $v=0$, 1, and 2 levels of the core. The fine structure is due to the interaction of the Rydberg electron with the ionic core.

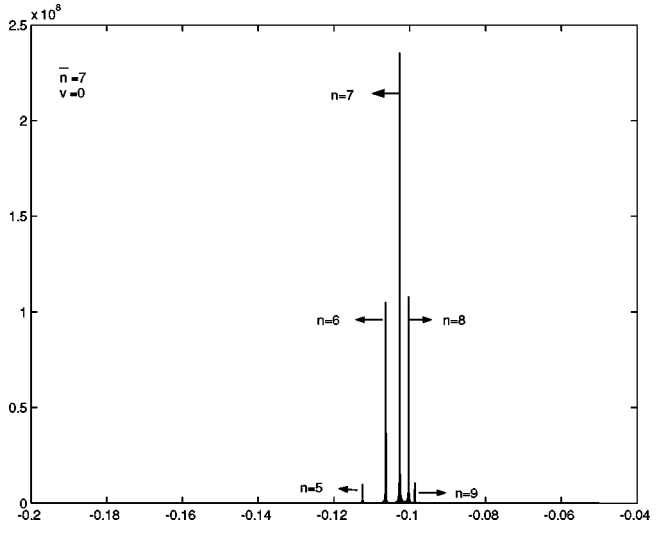


FIG. 5. Assigned Rydberg levels. The Rydberg series for $v=0$ in order of increasing $n$.

pling theory. Here we see three Ryderg series converging to the ground, the first, and the second excited vibrational states of the ion core, in accord with the initial vibrational wave packet that we created at $t=0$. In Fig. 5, we have assigned these energy levels in order of increasing $n$. When the energy levels, as predicted by average decoupling, are compared to unperturbed levels in Fig. 6 one sees a relative shift for $n=5$, which seems to disappear for $n=9$, in the corresponding line. This is in good agreement with the well known fact that the quadrupole energy shift, which has been directly worked into average decoupling theory, scales approximately as the inverse of $n^3l^3$.

## IV. ROTATIONS

When the barrier against rotations is lifted, new regions of configuration space will be accessible by the diatomic core, which has hitherto been approximated by a point quadrupole. Relative probabilities for arbitrary interacting configurations of the system will depend on the rotational state of the nuclei, thereby causing a delocalization of positions on the unit sphere which is difficult to model semiclassically (see Fig. 7). We can make progress by assuming that the rigid rotation is in a state with maximal angular momentum along the $z$ direction:

$$\psi_{rot}=Y_l^m(\theta,\phi), \quad l=m. \tag{41}$$

This confines the angular momentum onto a cone with very small apex angle, provided that $l$ is chosen sufficiently large. Moreover, the planar trajectories of the orbiting electron will, on average, experience zero torque[4] as any component of the

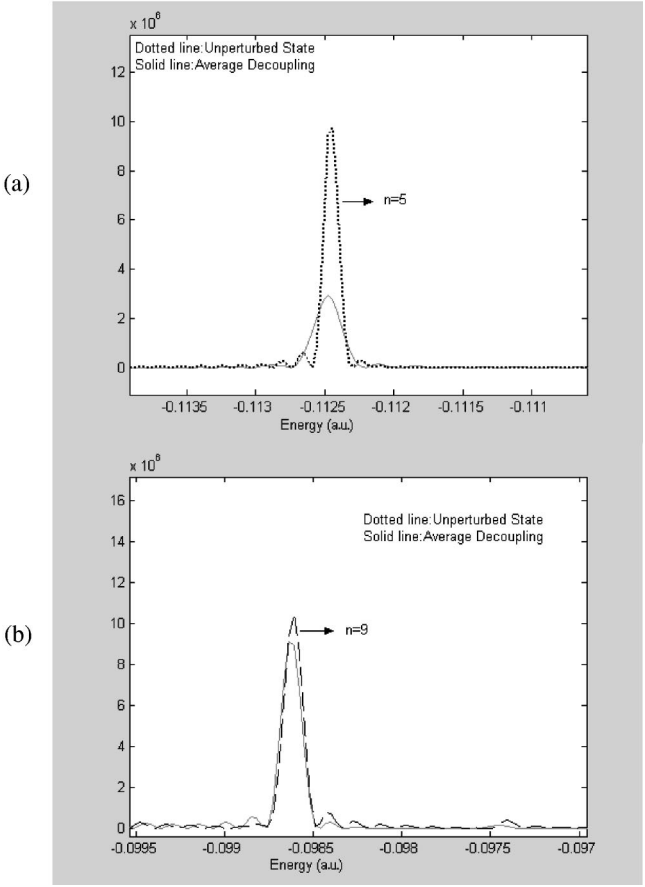


FIG. 6. Energy comparison. We observe here that the peak of the $n=5$ line computed using average decoupling theory has been shifted slightly to the left of the unperturbed state, implying an attractive ion-core–electron interaction. Such an energy shift is absent for the $n=9$ case. This implies that the nonspherical attraction between the core and the electron drops off very quickly with increased $n$ and $l$.

[4]This torque arises from the Coriolis and centrifugal forces, which are described by Eq. (59).

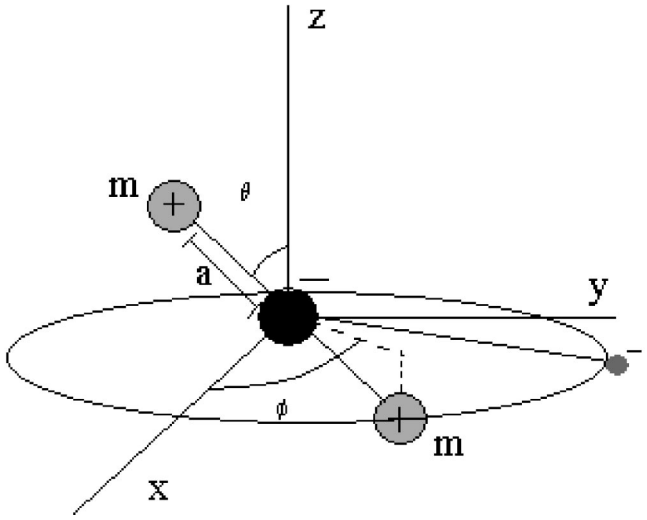


FIG. 7. Orientations of the rigid rotor on the unit sphere. Nuclear angular momentum is delocalized on the *x-y* plane where the classical electron trajectories lie. One can localize the nuclear rotation by letting the magnitude of the angular momentum be large and by maximizing the component along the *z* axis, i.e., $m=J$.

projection of the nuclear angular momentum on the plane of rotation of the electron will be canceled by the equally likely component lying along the axially opposite direction, as can be seen from Fig. 8.

In our sum over classical trajectories formula, the electronic motion is initiated in the asymptotic region and the electron remains on average at large distance from the center of the diatomic core due to its high angular momentum and the consequent centrifugal barrier. The signature for such motions is their long periods on the atomic scale. When the angular momentum quantum number is chosen to be large for the core rigid rotation, the nuclear motion becomes much faster than the electronic motion, i.e., the diatom completes many periods before the electron is able to complete one cycle. In this limit, the orbiting electron experiences a ring of charge near the origin, as opposed to two nuclei moving, and this is illustrated in Fig. 9. Following the usual convention, we decouple the rotations from vibrations by assuming that

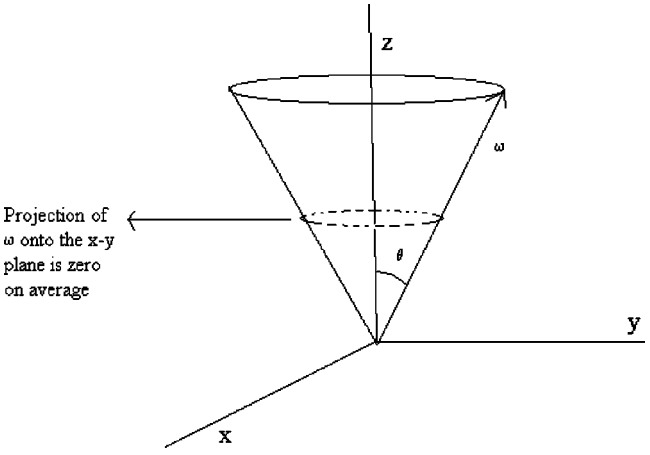


FIG. 8. Delocalization of angular momentum.

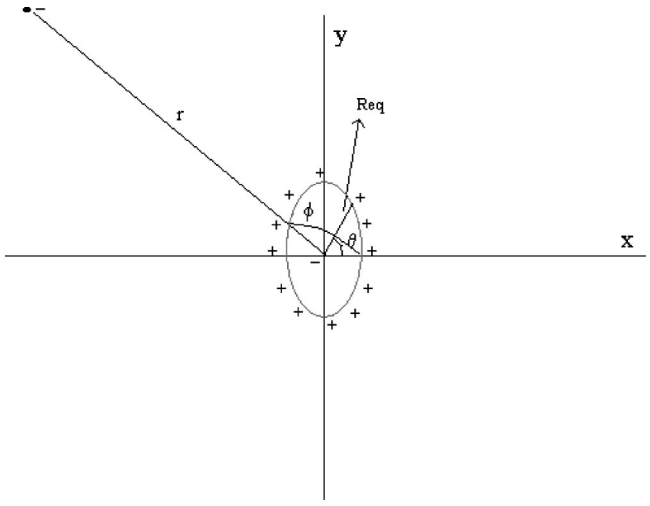


FIG. 9. Coplanar rotations of the core and the electron.

the moment of inertia remains on average the same, evaluated at the equilibrium bond length $U_{eq}$ during a period of the rotation. Thus, the result of allowing the nuclei to rotate is reduced to the multiplication of the autocorrelation function by an extra phase:

$$c(t)=c(t)^{*}e^{-iJ(J+1)t/2\mu U_{eq}^{2}}, \tag{42}$$

where $c(t)^{*}$ is the part that includes the electron dynamics coupled to rotations and $J$ is the rotational quantum number for the diatom. Next, we analyze the effects of the rotation-electronic couplings. The autocorrelation function has already been expressed as a sum over classical trajectories in Eq. (18). All we have to do now is to understand how the electron trajectories are modified by our present configuration involving a ring of charge near the origin. The total force experienced by an electron at position $\vec{r}$ becomes

$$\vec{F}=\oint \frac{\rho(\theta)(\vec{r}-\vec{R})dl}{(\vec{r}-\vec{R})^{3}}+\frac{1}{r^{2}}\hat{r}, \tag{43}$$

where, according to Fig. 9, $\vec{r}=r\cos(\phi)\hat{x}+r\sin(\phi)\hat{y}$ and $\vec{R}=U_{eq}\cos(\theta)\hat{x}+U_{eq}\sin(\theta)\hat{y}$. Explicitly,

$$\vec{F}=\rho U_{eq}\left[\int_{0}^{2\pi}\frac{[U_{eq}\cos(\theta)-r\cos(\phi)]d\theta\hat{x}}{[U_{eq}^{2}+r^{2}-2U_{eq}r\cos(\theta-\phi)]^{3/2}}+\int_{0}^{2\pi}\frac{[U_{eq}\sin(\theta)-r\sin(\phi)]d\theta\hat{y}}{[U_{eq}^{2}+r^{2}-2U_{eq}r\cos(\theta-\phi)]^{3/2}}\right]+\frac{1}{r^{2}}\hat{r}, \tag{44}$$

and the constant charge density on the ring is $\rho=1/\pi U_{eq}$. Since $U_{eq}\ll r$, we can series expand the denominators inside the integrands in powers of $U_{eq}/r$ to get

$$F_{x}=-\frac{\rho\pi(2r^{2}-3U_{eq}^{2})\cos(\phi)U_{eq}}{r^{4}}+\frac{\cos(\phi)}{r^{2}},$$

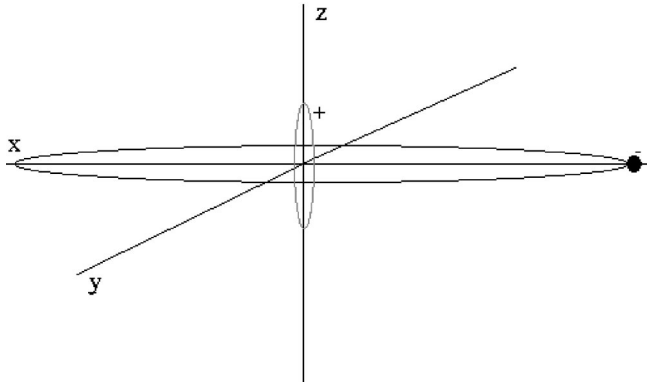


FIG. 10. Perpendicular rotations of the core and the electron. The electron rotates in the $x$-$y$ plane, whereas the nuclear rotation is in the $x$-$y$ plane.

$$F_y = -\frac{\rho\pi(2r^2 - 3U_{eq}^2)\sin(\phi)U_{eq}}{r^4} + \frac{\sin(\phi)}{r^2}. \quad (45)$$

This is a purely radial force and the equations of motion can be solved by circular orbits.[5] The new radii for these trajectories become

$$r_k(t) = \frac{(t/2\pi k)^{4/3} - U_{eq}^2}{(t/2\pi k)^{2/3}}. \quad (46)$$

This difference between Eq. (32) and Eq. (46) is the $U_{eq}^2$ term, which makes the new radii smaller. This shows that in this configuration there is an additional attractive interaction between the electron and the nuclei. The negative charge at the origin is shielded by the ring of positive charge and the effect of shielding increases as the radius of this ring increases. Since this radius is the internuclear separation, we can expect that the electron will be bound more strongly to the core as the internuclear separation increases, leading to a larger shift to lower energy in the corresponding electronic energy levels. Alternatively one could also choose to confine the angular momentum along the $x$ axis. This would imply that the nuclei and the electron are rotating in perpendicular planes, as in Fig. 10. Letting $\vec{r} = r\cos(\phi)\hat{x} + r\sin(\phi)\hat{y}$ and $\vec{R} = U_{eq}\cos(\theta)\hat{z} + U_{eq}\sin(\theta)\hat{y}$, we can carry out the integrations in Eq. (43) to get

$$F_x = -\frac{2\pi\rho\cos(\phi)U_{eq}}{r^2} + \frac{\cos(\phi)}{r^2},$$

$$F_y = -\frac{2\pi\rho\sin(\phi)U_{eq}}{r^2} + \frac{3\pi\rho}{r}\left(\frac{U_{eq}}{r}\right)^3\sin(\phi) + \frac{\sin(\phi)}{r^2}. \quad (47)$$

Here we have an asymmetry term in $\sin(\phi)$ of the order $(U_{eq}/r)^3$, which we will neglect because $U_{eq} \ll r$. In this limit, the total radial force experienced by the electron reduces to $F_r = -1/r^2$ and the electron trajectories are then given by Eq. (32). In this configuration, the shielding of the negative charge at the origin is reduced, leading to the disappearance of the attractive effect we observed in the case of

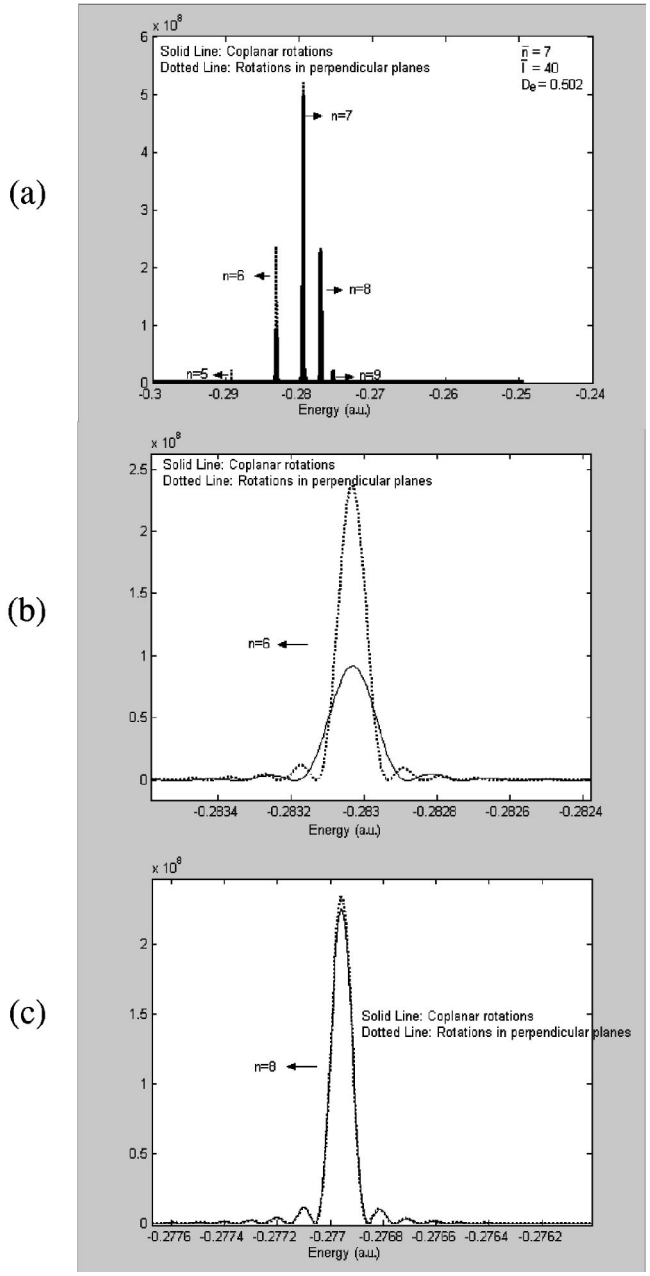


FIG. 11. Comparison of energy levels for coplanar vs perpendicular rotations. The solid line is coplanar rotations and the dashed line refers to perpendicular rotations. The parameters used are $J = 40$, $\bar{n} = 7$, $\mu = 918.01$, $k_{eff} = 0.3340$, $D_e = 0.502$, $U_{eq} = 2$, $\sigma_n = 10/(2\pi)$. It is observed in (b) that the energy peak for coplanar rotation is shifted slightly to the left of the peak for the perpendicular rotation, signifying that in the case of coplanar rotation the electron experiences stronger core attraction. As seen in (c), the difference in the two profiles vanishes when the principal quantum number gets large. At larger distances the electron is no longer affected by the ring structure of the core and therefore the overall attractive effect disappears.

[5] See Appendix A for mathematical details.

coplanar rotations. In a reference frame in which the position of the electron is fixed, the ring of charge makes a complete out-of-plane rotation during an electronic period, effectively forming a *sphere* of charge near the origin. The electric field outside the sphere reduces to the electric field produced by a point charge of magnitude $+1$ when the negative charge at the origin is also considered. Thus, the electronic motion becomes completely hydrogenlike. However, when the radius of the ring (the internuclear separation) is increased, the asymmetry term in Eq. (47) can no longer be neglected and the electron is pushed away from the core, settling into an elliptical orbit at higher energy. Hence, for this case of perpendicular rotation, the electron becomes less bound as the internuclear separation is increased. Having obtained the classical trajectories for the electron, the autocorrelation functions for the two cases of planar and perpendicular rotations can be computed, using the sum over classical trajectories formula in Eq. (15) with the same initial electronic wave function, and their Fourier transforms give the energy spectrum. In Fig. 11 we compare the energies for coplanar and perpendicular rotations. The parameters used are $\bar{n}=7$ and $J=40$. The depth of the potential energy curve has also been increased to $D_e=0.502$ to bind the extra rotational kinetic energy that we inject into rotations needed to confine the angular momentum along a specified axial direction. In this sense, our core is no longer explicitly $H_2^+$, but is an arbitrary diatomic core of total charge $+1$ and thus, as far as the motion of the Rydberg electron is concerned, can be approximated by a point quadrupole with a charge of $-1$ at the origin and two $+$ charges rotating about it. A closer look at the energy profiles in Fig. 11(b) displays the attractive effect of the coplanar rotations in contrast to the repulsive effect of perpendicular rotations for $n=6$. This effect seems to disappear in Fig. 11(c) as we go higher in the Rydberg series. This is well in agreement with our expectation that, when the electron principal quantum number increases, the average distance of the electron from the origin gets very large and the effect on the electron of the *ring* structure is no longer distinguishable from that of a point charge. Consequently, the relative shift in the energies vanishes.

#### Semiclassical rigid rotor and the stroboscopic effect

We can make the previous arguments more rigorous by explicitly treating the rotations of the nuclei semiclassically. If the autocorrelation function can be expressed as a sum over planar rotations, then average decoupling can more naturally be applied, since along every planar rotation of the rigid rotor, the rotor's angular momentum is well defined along the normal direction. However, due to the nature of the Hamiltonian, it is difficult to obtain an accurate semiclassical description for the rigid rotor. Satisfying results are obtained in the limit of high angular quantum number $J$ and heavier reduced mass $\mu$.

In the spirit of Sec. II, we begin by exciting a well localized rotational wave packet on the $x$-$y$ plane at $t=0$. This will allow us to express the autocorrelation function as a sum over classical rigid rotations within the $x$-$y$ plane. To achieve this, we choose as our initial wave packet a Gaussian superposition of spherical harmonics:

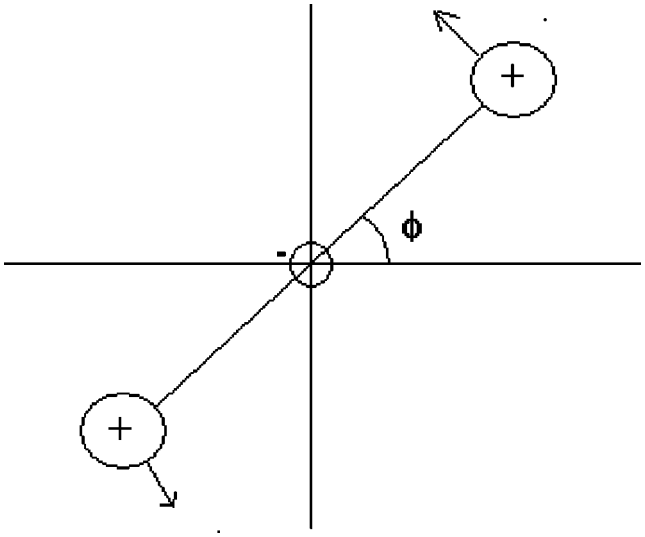


FIG. 12. Planar rotations in the $x$-$y$ plane.

$$\psi_0(\theta,\phi)=\sum_J a_J Y_{J,m}(\theta,\phi),$$

$$a_J=\left(\frac{1}{\pi\sigma^2}\right)^{1/4}\exp\left(\frac{-(J-\bar{J})^2}{2\sigma^2}\right), \quad J=m. \tag{48}$$

This wave packet has the property that $\bar{\theta}=\pi/2$ and $\bar{\phi}=0$ and $1\ll\bar{J}$. The autocorrelation function then becomes

$$c(t)=\int \psi_0(\theta_f,\phi_f,0)K(\theta_f,\phi_f,\theta_i,\phi_i,t) \times\psi_0(\theta_i,\phi_i,0)\sin\theta_f\sin\theta_i d\theta_f d\theta_i d\phi_f d\phi_i. \tag{49}$$

The classical Lagrangian for the system, according to Fig. 7, becomes

$$L=ma^2\dot{\theta}^2+ma^2\sin^2\theta\dot{\phi}^2, \tag{50}$$

where we let $m=2\mu$ and $U_{eq}=2a$. This leads us to the set of coupled differential equations:

$$ma^2\ddot{\theta}=ma^2\sin\theta\cos\theta\dot{\phi}^2,$$

$$\frac{d}{dt}(2ma^2\sin^2\theta\dot{\phi})=0. \tag{51}$$

Next we define the rotational angular momentum in the $\phi$ direction, which is conserved on every trajectory, as

$$2ma^2\sin^2\theta\dot{\phi}=p_\phi, \tag{52}$$

and substitution into Eq. (51) gives

$$\ddot{\theta}=\frac{\cos\theta}{4m^2a^4\sin^3\theta}p_\phi^2. \tag{53}$$

Planar solutions of these equations that lie in the $x$-$y$ plane can be written as (see Fig. 12)

$$\phi(t') = \frac{p_\phi}{2ma^2}t' + \phi_i, \qquad \theta(t') = \theta_i. \tag{54}$$

The mapping into quantum mechanics is achieved by considering the stability properties of these trajectories via the partial derivative matrices of the action. To calculate these matrices we consider, instead, a particular set of solutions in which there are small oscillations about the equilibrium $\theta$ position:

$$\phi(t') = \frac{p_\phi}{2ma^2}t' + \phi_i, \tag{55}$$

$$\theta(t') = \theta_i + \frac{p_\theta^i}{p_\phi}\sin\left(\frac{p_\phi}{2ma^2}t'\right),$$

where $p_\theta^i$ is the initial rotational angular momentum in the $\theta$ direction. It is now straightforward to calculate the partial derivatives of the action, which then constitute the blocks of the monodromy matrix [6]. The monodromy matrix can then be utilized to calculate the integral in Eq. (15), and the resulting expression can finally be evaluated[6] at the planar orbit given in Eq. (54) with $\theta_i = \pi/2$, $\phi_i = 0$, $p_\phi/2ma^2 = 2\pi j/t$, and $j$ is an integer.

The final form for the autocorrelation function is

$$c(t) = \sum_j \frac{\exp[-1/2ij\pi - \bar{J}^2/\sigma^2 - 16a^4j^2m^2\pi^2/\sigma^2t^2 + 4a^2jm\pi(ij\pi + 2\bar{J}/\sigma^2)]}{\sqrt{1 + it\sigma^2/4a^2m}}. \tag{56}$$

Here the classical action is $R_{rot}^j = ma^2 4\pi^2 j^2/t$ and the index $j$ refers to summations over planar rotations with circular frequency $\omega_j = 2\pi j/t$. The exact autocorrelation function is given by

$$c(t) = \sum_J |a_J|^2 e^{-iJ(J+1)/2\mu U e q^2}. \tag{57}$$

In Fig. 13 we compare the exact result to the semiclassical result. The parameters were taken to be $\bar{J} = 50$ and $\mu = 3200$ a.u. It is seen that the semiclassical approximation is quite accurate over a time length of 15 classical rotational periods, where a classical rotation period is given by $T_{rot} = 2\pi\mu U_{eq}^2/\bar{J}$.

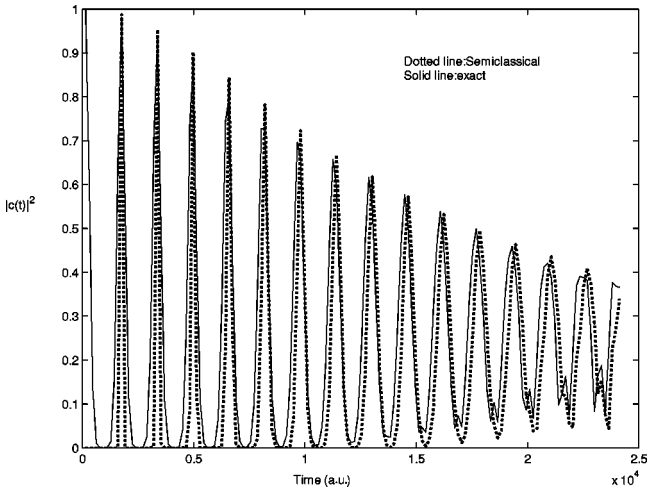


FIG. 13. Accuracy of the semiclassical rigid rotor. The solid line is the exact result and the dotted line refers to the semiclassical approximation. The parameters used are $\bar{J} = 50$, $\mu = 3200$, $U_{eq} = 2$, $\sigma = 10/(2\pi)$.

Armed with this result, we return to the case of the diatom with an orbiting Rydberg electron. Over a rotation of the diatomic core, the positive nuclei interact with the Rydberg electron in orbit through long range interactions. We can model the effect of this rotation on the electronic motion by describing it in a rotating frame of reference with circular frequency $\omega_j$. This follows from the average decoupling formula in Eq. (18), which generalizes as

$$c(t) = \sum_j a_j e^{iR_{rot}^j} \sum_k b_{kj} e^{iR_{el,j}^k} \int \psi_{vib}^* K_{jk} \psi_{vib} dR, \tag{58}$$

where $a_j$ is obtained from Eq. (56), $R_{el,j}$ is the electronic action, $K_{jk}$ is the vibrational propagator, and the subscript $j$ in the remaining terms signifies that the electronic and vibrational parameters are evaluated inside the $j$th rotating frame of reference. What remains to be done is to understand how the electronic trajectories get modified inside a rotating frame. The equation of motion of an electron inside a frame that rotates along $\vec{\omega}_j$ becomes

$$\frac{d^2\vec{r}}{dt^2} = -\frac{1}{r^2}\hat{r} - 2\vec{\omega}_j \times \frac{d\vec{r}}{dt} - \vec{\omega}_j \times (\vec{\omega}_j \times \vec{r}), \tag{59}$$

where the additional two terms are known as the Coriolis and centrifugal forces, respectively. By the nature of the initial rotational wave packet we choose to excite, we have $\vec{\omega}_j$

[6] See Appendix B for the full derivation.

$=\omega_j\hat{z}$. We can, however, reverse the direction of this vector by making the substitution $m\mapsto -m$ in the initial rotational wave packet, where $m$ is the magnetic quantum number. From this point on, we consider both orientations simultaneously. Since the rotation vector points in the direction normal to the plane of motion of the electron, Eq. (59) can still be solved with Kepler orbits, and the new radii for the circular electron trajectories in the rotating frame become

$$r_{jk}^{\pm}(t)=\frac{1}{|2\pi j/t\pm 2\pi k/t|^{2/3}}, \tag{60}$$

in contrast to Eq. (32). Here $\omega_{el}=2\pi k/t$ are the electron frequencies inside the rotating frame of reference. The $+$ sign in Eq. (60) is used to signify that the nuclei and the electron rotate in the same direction whereas the $-$ sign refers to the nuclei and electron rotating in opposite directions. Using this new definition for $r_k$, we can now go back and reevaluate the atomic term $\Omega(k)$ of Eq. (30). Clearly the $\pm$ sign that appears in the definition of $r_k$ leads to different modifications of the autocorrelation function. This serves to break the degeneracy in the electronic motion reflecting its orientation relative to the nuclear angular momentum. Next, we account for the vibrations. In the rotating frame, the time derivative of the vector $\vec{U}$ that connects the two nuclei is given by

$$\frac{d\vec{U}}{dt}=\dot{\vec{U}}+\omega_j\times\vec{U}. \tag{61}$$

Here $\dot{\vec{U}}$ is the rate of change of the vector $\vec{U}$ as measured inside the rotating frame. This makes an additional contribution to the kinetic energy in the Lagrangian which can approximately be taken as

$$E_o^j=\frac{1}{2}w_j^2U_{eq}^2. \tag{62}$$

Therefore the immediate effect of rotations on the vibrations is an upward shift of the zero of energy. The average force constant of Eq. (28) models the coupling of the vibrational motion to the electronic motion. Its explicit form depends on the trajectory of the electron, and in the simple case of circular orbits, the radius of the circle. Using Eq. (60) in Eq. (28), we can then account for the electronic-vibrational coupling inside the rotating frame of reference. The average vibrational force constant becomes

$$g_{kj}^{\pm}=\frac{-|2\pi j/t\pm 2\pi k/t|^2t}{4}+k_{eff}. \tag{63}$$

We are now in a position to express the complete autocorrelation function for the system using Eqs. (60), (34), (63), (56), and (58). For the initial wave packet,

$$\begin{aligned}
&\psi(0)=\psi_{rot}\psi_{el}\psi_{vib},\\
&\psi_{rot}(\theta,\phi)=\frac{1}{\sqrt{2}}\sum_J a_J Y_{J,m}(\theta,\phi)\\
&\qquad\qquad+\frac{1}{\sqrt{2}}\sum_J a_J Y_{J,-m}(\theta,\phi),\\
&\psi_{el}(\vec{r},0)=\sum_n\left(\frac{1}{\pi\sigma_n^2}\right)^{1/4}e^{-(n-\bar{n})^2/2\sigma_n^2}\phi_{n,n-1,n-1},\\
&\psi_{vib}(R)=\psi_o^{HO}.
\end{aligned} \tag{64}$$

The semiclassical autocorrelation function can be written as

$$\begin{aligned}
c(t)=&\frac{1}{2}\sum_j\sum_k a_j\Omega_j^+(k)\exp\left\{-it\left[\frac{1}{2}\sqrt{\frac{g_{jk}^+}{\mu}}+\frac{k_{eff}U_{eq}^2(g_{jk}^+-k_{eff})}{2g_{jk}^+}-D_e+\frac{1}{2}\left(\frac{2\pi j}{t}\right)^2U_{eq}^2\right]\right\}+\frac{1}{2}\sum_j\sum_{k\neq j}a_j\Omega_j^-(k)\\
&\times\exp\left\{-it\left[\frac{1}{2}\sqrt{\frac{g_{jk}^-}{\mu}}+\frac{k_{eff}U_{eq}^2(g_{jk}^--k_{eff})}{2g_{jk}^-}-D_e+\frac{1}{2}\left(\frac{2\pi j}{t}\right)^2U_{eq}^2\right]\right\},
\end{aligned} \tag{65}$$

$$a_j=\frac{\exp\left[-\frac{1}{2}ij\pi-\bar{J}^2/\sigma^2-16a^4j^2m^2\pi^2/\sigma^2t^2+4a^2jm\pi(ij\pi+2\bar{J}/\sigma^2)\right]}{\sqrt{1+it\sigma^2/4a^2m}},$$

$$\Omega_j^{\pm}(k)=\frac{1}{\sigma_n\sqrt{(1/\sigma_n)^2-i3t/2r_{kj}^{\pm}}}\exp\left[-\frac{(\sqrt{r_{kj}^{\pm}}-\bar{n})}{\sigma_n^2+i2(r_{kj}^{\pm})^2/3t}+i\left(2\pi k\sqrt{r_{kj}^{\pm}}+\frac{t}{2r_{kj}^{\pm}}\right)\right],$$

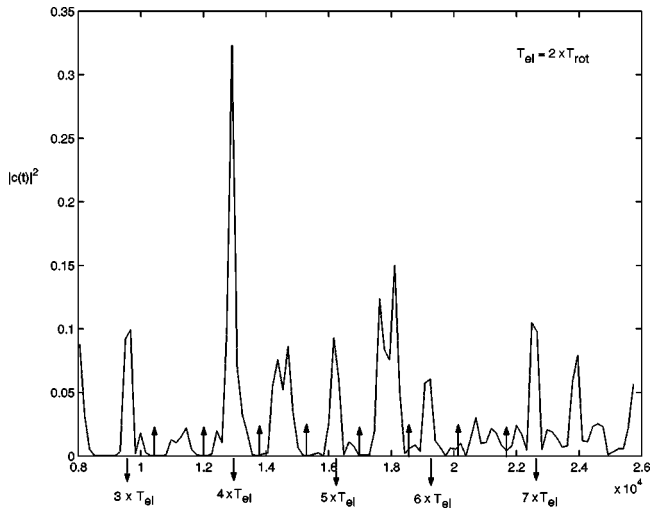


FIG. 14. Recurrence spectrum. The parameters used are $\bar{J}=50$, $\bar{n}=8$, $\mu=3200$, $k_{eff}=0.3340$, $D_e=0.502$, $U_{eq}=2$, $\sigma_n=\sigma=10/(2\pi)$. The signature of the stroboscopic effect can be seen at the points marked by the arrows.

and is plotted in Fig. 14. The parameters used were $\bar{J}=50$, $\bar{n}=8$, $\mu=3200$ a.u., $D_e=0.502$. These values were chosen so that the special condition of $2\pi\bar{n}^3=2T_{rot}$ was achieved. In other words the classical period of rotation of the electron was fixed to be twice the classical period of rotation of the nuclei, thus tuning the two motions into resonance.

It is known that in the recurrence spectrum of atomic hydrogen, peaks are observed at times corresponding to integer multiples of the Kepler periods. Such peaks are also seen in Fig. 14. The positions marked with the downward pointing arrows correspond to integer multiples of the classical electronic period and thus even integer multiples of the rotational period. Partial recurrences are repeated consistently at these points. However, if the points at about a quarter of the electronic period away from the downward pointing arrows are investigated,[7] it is seen that recurrences completely vanish and the survival probability almost drops to zero. This behavior can be explained by considering classical configurations of the electron-diatom system. At integer multiples of the electronic periods the two motions are in phase. The electron starts out with the nuclei at a certain orientation, completes a period, and comes back to find the nuclei in the same orientation. It is as if the nuclei have not moved at all [Fig. 15(a)]. However, at the points when the survival probability is approaching zero, the classical motions are out of phase. In other words, at these points the electron completes about a quarter of its period whereas the nuclei are able to go through half a period [Fig. 15(b)]. The electron is affected by the opposite of the orientation from which it started, leading to destructive interference in the corresponding wave mechanics that describe the two motions. Thus the survival probability approaches zero. However, if the electron is allowed to traverse an additional quarter of a period, it will find itself in its original configuration once again, and this is indeed manifested in the figure by further partial recurrences at the midpoints of the downward pointing arrows. If the autocorrelation function is considered as a probe of the state of a system, then the situation can be related to a classical system such as a weakly coupled pendulum-oscillator pair inside a completely dark room. The probe in this case will be a light switch that we can turn on at times we choose to observe the state of the system, but we cannot keep the light on continuously. Now suppose that the period of small oscillations of the pendulum is twice that of the oscillator. Then if we turn on the light switch at times corresponding to integer multiples of the period of the pendulum, we will not be able to tell if the system has moved at all as both the oscillator and the pendulum will be back at their original positions. Only if we come in at the correct times, i.e., the times at which the two motions are out of phase, will we be able to observe motion. This is known as the *stroboscopic* effect. Our autocorrelation function displays a direct manifestation of the stroboscopic effect in the realm of quantum mechanics which was first suggested by [9].

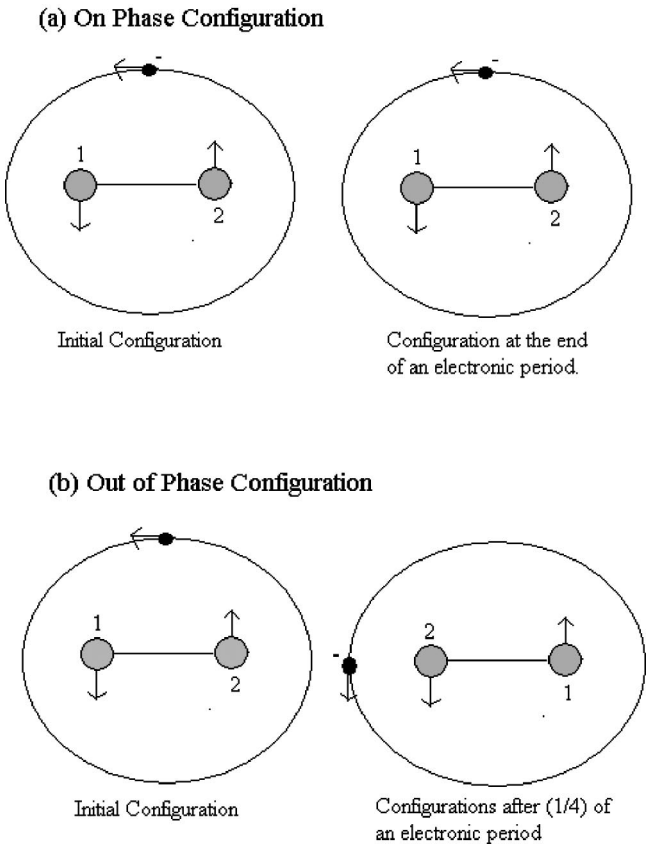


FIG. 15. Classical configurations.

## V. CONCLUSION

We have given a semiclassical treatment of Rydberg dynamics for a well localized initial wave packet in a diatomic system. It has been shown that our sum over classical orbits

[7]These are marked with upward pointing arrows in the figure.

formula allows us to decouple the vibration-electronic interaction, based upon an averaging principle derived primarily from a classical model. Our results agree well with the predictions of a perturbation theory treatment of the same problem. Inclusion of the rotations took place in two steps. In the first step, we worked in the limit of the nuclei moving much faster than the Rydberg electron. This has led to the introduction of an approximation of the free rotation of the nuclei by a ring of charge placed near the origin in order to analyze the dynamics of the electron. The approximation correctly predicted how the energies for the electron will be shifted, based upon the relative orientations of the two motions in the sense of coplanar versus perpendicular rotations. In the second step, we worked in the limit of resonance in which the average period for rotation matched an integer multiple of the average electronic period. Consequently, we recovered partial recurrences in the survival probability. These recurrences are the signature of the stroboscopic effect that arises when two separate parts of a system move in resonance. This illustrates how the classical concept of resonance maps into the dynamics of a fundamentally quantum mechanical molecular system.

## ACKNOWLEDGMENTS

This research was supported by NSF Grant Nos. CHE-0104197 and CHE-009321. S.N.A. is grateful for support by MIT.

## APPENDIX A

For the case of coplanar rotations we solve the equations of motion for the electron with reference to Fig. 9. The total force experienced by the electron located at $\vec{r}$ is given by

$$\vec{F}=\oint \frac{\rho(\theta)(\vec{r}-\vec{R})dl}{(\vec{r}-\vec{R})^3}+\frac{1}{r^2}\hat{r}. \tag{A1}$$

Explicitly,

$$\vec{F}=\rho U_{eq}\left[\int_0^{2\pi}\frac{[U_{eq}\cos(\theta)-r\cos(\phi)]d\theta\hat{x}}{[U_{eq}^2+r^2-2U_{eq}r\cos(\theta-\phi)]^{3/2}} + \int_0^{2\pi}\frac{[U_{eq}\sin(\theta)-r\sin(\phi)]d\theta\hat{y}}{[U_{eq}^2+r^2-2U_{eq}r\cos(\theta-\phi)]^{3/2}}\right]+\frac{1}{r^2}\hat{r}. \tag{A2}$$

Taylor expansion to second order in $U_{eq}/r$ gives

$$\frac{1}{[U_{eq}^2+r^2-2U_{eq}r\cos(\theta-\phi)]^{3/2}} \rightarrow \frac{1+3\cos(\theta-\phi)U_{eq}/r}{r^3}, \tag{A3}$$

which leads to

$$F_x=-\frac{\rho\pi(2r^2-3U_{eq}^2)\cos(\phi)U_{eq}}{r^4}+\frac{\cos(\phi)}{r^2},$$

$$F_y=-\frac{\rho\pi(2r^2-3U_{eq}^2)\sin(\phi)U_{eq}}{r^4}+\frac{\sin(\phi)}{r^2}. \tag{A4}$$

The total central force becomes

$$\vec{F}=-\frac{r^2-3U_{eq}^2}{r^4}\hat{r}, \tag{A5}$$

which leads to the equation

$$\frac{4\pi^2k^2}{t^2}=\frac{r^2-3U_{eq}^2}{r^5}. \tag{A6}$$

The solution we are looking for corresponds to a root of

$$ar^5-r^2+3U_{eq}^2=0,$$

$$a=\frac{4\pi^2k^2}{t^2}. \tag{A7}$$

The equation for the approximating line to the curve $ar^5-r^2+3U_{eq}^2$ passing from the point $((1/a)^{1/3},3U_{eq}^2)$ is given by

$$y=3\left(\frac{1}{a}\right)^{1/3}r+3\left[U_{eq}^2-\left(\frac{1}{a}\right)^{2/3}\right], \tag{A8}$$

which intersects the $r$ axis at the point

$$r_k=\frac{(1/a)^{2/3}-U_{eq}^2}{(1/a)^{1/3}}. \tag{A9}$$

For the case of perpendicular rotations we refer to Fig. 10. The expression in Eq. (A1) becomes

$$\vec{F}=\rho U_{eq}\left[\int_0^{2\pi}-\frac{r\cos(\phi)d\theta\hat{x}}{(U_{eq}^2+r^2-2U_{eq}r\sin\phi\sin\theta)^{3/2}} + \int_0^{2\pi}\frac{[U_{eq}\sin(\theta)-r\sin(\phi)]d\theta\hat{y}}{(U_{eq}^2+r^2-2U_{eq}r\sin\phi\sin\theta)^{3/2}} + \int_0^{2\pi}\frac{U_{eq}\cos\theta d\theta\hat{y}}{(U_{eq}^2+r^2-2U_{eq}r\sin\phi\sin\theta)^{3/2}}\right]+\frac{1}{r^2}\hat{r}. \tag{A10}$$

The third of these integrals vanishes. Taylor expansion in $U_{eq}/r$ to second order gives

$$\frac{1}{(U_{eq}^2+r^2-2U_{eq}r\sin\theta\sin\phi)^{3/2}} \rightarrow \frac{1+3\sin\theta\sin\phi U_{eq}/r}{r^3}, \tag{A11}$$

which then leads to

$$F_x=-\frac{2\pi\rho\cos(\phi)U_{eq}}{r^2}+\frac{\cos(\phi)}{r^2},$$

$$F_y=-\frac{2\pi\rho\sin(\phi)U_{eq}}{r^2}+\frac{3\pi\rho}{r}\left(\frac{U_{eq}}{r}\right)^3\sin(\phi)+\frac{\sin(\phi)}{r^2}. \tag{A12}$$

## APPENDIX B

Planar solutions of the equations of motion for the rigid rotor are given by

$$\phi(t')=\frac{P_\phi}{2ma^2}t'+\phi_i,$$

$$\theta(t')=\theta_i.$$

To calculate the stability properties of these trajectories we consider small oscillations about $\theta_0$. We let

$$\theta(t')=\theta_i+\epsilon(t'),$$

where $\epsilon(t')$ is small. Substitution into Eq. (53) and Taylor expansion to first order in $\epsilon$ gives

$$\ddot{\epsilon}=-\frac{p_\phi^2}{4m^2a^4}\epsilon.$$

The solutions subject to the initial conditions

$$\theta(0)=\theta_i,$$

$$\dot{\theta}(0)=p_\theta^i,$$

are given in Eq. (55). Considering small oscillations about $\theta_i$ reduces the blocks of the monodromy matrix to diagonal form. The monodromy matrix in this limit is given by

$$\begin{pmatrix} \frac{\partial\vec{q}_f}{\partial\vec{q}_i} & \frac{\partial\vec{q}_f}{\partial\vec{p}_i} \\ \frac{\partial\vec{p}_f}{\partial\vec{q}_i} & \frac{\partial\vec{p}_f}{\partial\vec{p}_i} \end{pmatrix}=\begin{pmatrix} A & B \\ C & D \end{pmatrix},$$

with

$$A=\begin{pmatrix}1&0\\0&1\end{pmatrix},\quad B=\begin{pmatrix}\sin\left(\frac{P_\phi t}{ma^2}\right)/p_\phi & 0\\ 0 & \frac{ma^2}{t}\end{pmatrix},$$

$$C=\begin{pmatrix}0&0\\0&0\end{pmatrix},\quad D\begin{pmatrix}1&0\\0&1\end{pmatrix}.$$

Defining further the matrices

$$\sigma=\begin{pmatrix}\sigma&0\\0&\sigma\end{pmatrix},\quad K=i\sigma^{-2},$$

$$S=\begin{pmatrix}2 & 0\\ 0 & 2+\frac{it}{2a^2m\sigma^2}\end{pmatrix},$$

$$T=\begin{pmatrix}1 & 0\\ 0 & 1+\frac{it}{2a^2m\sigma_2}\end{pmatrix},$$

and the vectors

$$\vec{p}_l=\begin{pmatrix}0\\ l\end{pmatrix},\quad \vec{p}_0=\begin{pmatrix}0\\ p_\phi\end{pmatrix},$$

we can carry on the integration given in Eq. (15) to get

$$c=\sum_j a_j,$$

$$a_j=|\det(S/2)|^{1/2}\times\exp\left(iR_j-i\frac{\pi}{2}\mu_j-\sigma(\vec{p}_0-\vec{p}_l)TS^{-1}\sigma(\vec{p}_0-\vec{p}_l)+\sigma(\vec{p}_0-\vec{p}_1)S^{-1}\sigma(\vec{p}_0-\vec{p}_1)\right).$$

Here the final expression is evaluated over a planar rotation on the $x$-$y$ plane for which we have

$$p_\phi=\frac{2\pi jma^2}{t},\quad R_j=ma^2\frac{4\pi^2j^2}{t},$$

and the number of conjugate points is given by

$$\mu_j=j,$$

corresponding to $j$ crossings through the $\theta$ axis of the oscillating sine term over its $j$ periods.[8]

[8]See Refs. [4] and [5] for further information on multidimensional Gaussian integrations.

[1] M. Mallalieu and C. R. Stroud, Phys. Rev. A **49**, 2329 (1994).
[2] W. Kolos and L. Wolniewicz, Rev. Mod. Phys. **35**, 473 (1963).
[3] O. Atabek and C. H. Jungen, J. Chem. Phys. **66**, 5584 (1977).
[4] V. G. Stavros, J. A. Ramswell, R. A. L. Smith, J. R. R. Verlet, J. Lei, and H. H. Fielding, Phys. Rev. Lett. **83**, 2552 (1999).
[5] C. Goldstein, *Classical Mechanics* (Addison-Wesley, Reading, MA, 1980).
[6] M. C. Gutzwiller, *Chaos in Classical and Quantum Mechanics* (Springer-Verlag, New York, 1990).
[7] M. Naunberg, Phys. Rev. A **40**, 1133 (1989).
[8] Z. D. Gaeta and C. R. Stroud, Phys. Rev. A **42**, 6308 (1990).
[9] P. Labastie, M. C. Bordas, B. Tribollet, and M. Broyer, Phys. Rev. Lett. **52**, 1681 (1984).